

Wintertime Simulations of a Boreal Lake with the Canadian Small Lake Model

MURRAY D. MACKAY

Meteorological Research Division, Environment and Climate Change Canada, Toronto, Ontario, Canada

DIANA L. VERSEGHY

Climate Research Division, Environment and Climate Change Canada, Toronto, Ontario, Canada

VINCENT FORTIN

Meteorological Research Division, Environment and Climate Change Canada, Toronto, Ontario, Canada

MICHAEL D. RENNIE

Lakehead University, Thunder Bay, Ontario, and IISD Experimental Lakes Area, Winnipeg, Manitoba, Canada

(Manuscript received 14 November 2016, in final form 17 May 2017)

ABSTRACT

A one-dimensional mixed layer dynamic lake model is enhanced with snow and ice physics for an examination of processes governing ice cover and phenology in a small boreal lake. The complete snowpack physics module of the Canadian Land Surface Scheme along with a new snow-ice parameterization have been added to the Canadian Small Lake Model, and detailed meteorological and temperature profile data have been acquired for the forcing and evaluation of two wintertime simulations. During the first winter, simulated ice-on and ice-off biases were -3 and -5 days, respectively. In the second winter simulation, ice-on bias was larger, likely due to the absence of a frazil ice scheme in the model, and simulated ice-off was 6 days late, evidently due to insufficient convective mixing beneath the ice in the weeks leading up to ice-off. Ice cover was simulated about 25% too thin between January and March for this year, though late January simulated snow and snow-ice amounts were close to observed. The impact of snow-ice production on simulated ice cover and phenology was found to be dramatic for this lake. In the absence of this process, January snow was more than twice as deep as observed and March ice thickness was less than one-third of that observed. Without snow-ice production, a reasonable simulation of ice cover could only be restored if 62% of snowfall was removed ad hoc (e.g., through blowing snow redistribution)—an excessive amount for a small, sheltered boreal lake.

1. Introduction

There is by now a general recognition that lakes are important components of the climate system through the flux exchange of heat, moisture, radiation, and trace gases. All of these fluxes are strongly affected by the presence and nature of snow and ice cover, so it is essential to model snow and ice processes well in lake models that are coupled with Earth system models in studies of global and regional climate. It is equally important to model snow and ice cover well in studies of aquatic ecosystems. Ice phenology, for example, plays an important role in the timing and duration of the summer

stratified period and thus the life cycle of cold water stenotherms. In addition, the length of the ice-free season determines the cumulative ultraviolet B (UVB) exposure organisms would face. During winter, light availability under ice is strongly affected by ice and snow thickness, which has important implications for nutrient cycling. Ice cover duration also impacts anaerobic mineralization processes and thus nutrient availability and trace gas accumulation. All of these issues are particularly important at high latitudes (MacKay et al. 2009). It is clear that ice cover duration, ice-on and ice-off dates, and ice and snow thickness are important to understand and model well for the climate analyst and limnologist alike.

Most small lake models of the type used in studies of climate and climate change have schemes to develop ice cover and at least rudimentary snow processes. In

Corresponding author: Murray MacKay, murray.mackay@canada.ca

regions with significant snowfall, the production of snow-ice can be an important contribution to total ice cover (e.g., Kirillin et al. 2012), though this is not always included in models. Snow-ice forms when the weight of the overlying snow exceeds the carrying capacity of the ice, which then cracks to allow lake water to flood the bottom of the snow layer to form slush. Note that a slush layer can also form when rain or snowmelt percolates to the bottom of the snow layer. Under appropriate conditions, the slush layer freezes to form a layer of white ice that is generally less dense and more opaque than congelation (or black) ice.

Though by no means universal, a number of small lake models do attempt to incorporate this process. For example, Patterson and Hamblin (1988) represented snow-ice production in the Dynamic Reservoir Simulation Model (DYRESM) by simply converting excess snow cover (i.e., in excess of the ice carrying capacity) directly into snow-ice, evidently disregarding the energetics of the process. Studies using the Lake Ice Model Numerical Operational Simulation (LIMNOS; e.g., Vavrus et al. 1996; Elo and Vavrus 2000) also took this approach. Rogers et al. (1995) improved on this by computing the heat released during snow-ice production (which they found to be significant) in their version of DYRESM and distributing it throughout the snowpack. In their calculation, they include the latent heat of fusion for the freezing pore water as well as the heat introduced by the flooding lake water, but they disregard the temperature of the flooded snow layer. While the flooding lake water is likely close to the freezing point already, the snow itself can be very cold. In addition, their scheme does not account for the thermal expansion of the freezing slush layer. Oveisly and Boegman (2014) employed the same snow-ice scheme in their version of DYRESM. None of the above studies of DYRESM and LIMNOS evaluated the simulation of snow-ice in particular, though they did examine snow and ice evolution. LIMNOS was found to reproduce ice-on and ice-off dates generally within a week. Ice phenology was not evaluated in the above studies of DYRESM, though more recently de Stasio et al. (2016) reported mean ice-on and ice-off biases of 5 and 9 days, respectively, in a 23-yr simulation of their version of DYRESM (though for some years the bias was more than 3 weeks), and Magee et al. (2016) found mean absolute errors in ice-on and ice-off to be 2 and 6 days, respectively, in their 104-yr simulation.

Thermodynamic lake ice models with simplified lower boundary conditions, but which represent snow-ice production include the High Resolution Thermodynamic Snow and Ice (HIGHTSI) model and the Canadian Lake Ice Model (CLIMo). HIGHTSI (e.g., Yang

et al. 2012; Semmler et al. 2012) includes detailed snow and ice process physics but represents the underlying lake [or ocean, as in Cheng et al. (2003)] by a fixed, specified heat flux. Snow-ice can form when the lower snowpack is flooded as above, though the procedure only approximately conserves energy and does not include the thermal expansion of freezing slush (Cheng et al. 2003). Neither study compares phenology with observations in any detail, but Yang et al. (2012) suggest that the ice-off date was “close to the observation” in a 1-yr case study (apparently within a day or two). They do note, however, that both the simulated maximum ice thickness and ice-off date were sensitive to the specified water-to-ice heat flux required by the model in the absence of an underlying lake model. Snow-ice was simulated, and observed, to be at most a few centimeters in their study—unfortunately, not a very robust test for their scheme. Semmler et al. (2012) did not have any snow-ice observations for direct comparison in their 1-yr simulation, but they did find a significant improvement in total ice thickness when their snow-ice scheme was turned on.

CLIMo (Duguay et al. 2003; Ménard et al. 2002) also includes physical processes for snow and ice, but it represents the underlying lake with a simple isothermal mixed layer. When ice is absent, this model simulates an evolving lake temperature based on the surface energy balance, but in the presence of ice the mixed layer is fixed at the freezing point. This approach does not represent thermal stratification beneath the ice cover, nor the radiative warming and mixing of near-surface water in the spring before ice-off (e.g., Keitzl et al. 2016; Mironov et al. 2002). Patterson and Hamblin (1988) argue that under-ice convective mixing bringing relatively warm water up to the bottom ice surface is in fact the most important mechanism leading to ice-off. Snow-ice production in CLIMo is as in Flato and Brown (1996). Biases in ice phenology are generally reported to be from a few days to a week, but both ice-off date and ice thickness are sensitive to the specified snow cover scenario used (Duguay et al. 2003; Kheyrollah Pour et al. 2012). Thus, the lack of under-ice springtime convective mixing in HIGHTSI and CLIMo, as far as ice-off is concerned, could be compensated for by adjusting the water-to-ice heat flux or removing snow cover, respectively.

Recently, the snow cover physics package of the Canadian Land Surface Scheme (CLASS), the land surface component of the Second Generation Canadian Earth System Model (CanESM2), has undergone extensive validation (Verseghy et al. 2017). In this study, these routines, as well as a new scheme for snow-ice production, have been added to the Canadian Small Lake Model (CSLM; MacKay 2012), and two wintertime

simulations of a small boreal lake at the Experimental Lakes Area (ELA) of northwestern Ontario, Canada, are examined. Carefully constructed meteorological forcing and evaluation data along with sensitivity experiments help elucidate important physical processes and demonstrate the model's suitability for fully coupled climate and environmental prediction applications. In section 2 enhancements to the model and details of the forcing and evaluation data are described, section 3 presents results for two wintertime simulations, section 4 discusses some sensitivity experiments with the model, and a general discussion ensues in section 5, with conclusions presented in section 6.

2. Method

a. Model description

Version 1 of the CSLM is fully described in MacKay (2012), where the focus was largely on summertime processes, especially mixed layer deepening. Here we briefly reiterate the relevant mixed layer dynamics, describe in more detail the formation of ice, and introduce new schemes for snow cover and snow-ice production.

1) EQUATION OF STATE AND THE MIXED LAYER MODEL

The equation of state follows Farmer and Carmack (1981), except that we neglect pressure and salinity effects. Thus,

$$\rho = \rho_0(1 - \beta\hat{T}^2) \quad \text{and} \\ \hat{T} = T - T_M,$$

where ρ is the density, T is the temperature, T_M is the temperature of maximum density, ρ_0 is the maximum density of pure water at atmospheric pressure, and β is a constant. Thus, \hat{T} is the departure from the temperature of maximum density and can be positive or negative for liquid water. As in Farmer and Carmack (1981), we choose $\rho_0 = 999.975 \text{ kg m}^{-3}$, $\beta = 8.2545 \times 10^{-6} \text{ C}^{-2}$, and $T_M = 3.983^\circ\text{C}$. Incorporating (weak) salinity would essentially change the values of ρ_0 and T_M , and including the effects of pressure would add a term linear in \hat{T} to the density equation. However, the most important feature in this equation of state for our purposes is the quadratic dependence on T that allows for the lake to restratify prior to ice-on once the lake has cooled below T_M . Free convection (gravitational instability) occurs whenever dense water overlies lighter water in adjacent layers. Under these conditions, layers are successively mixed until a stable density profile ensues. This process occurs throughout the cooling phase of the lake, including when

near-surface water that has cooled below T_M is subject to shortwave radiation. This is of particular interest during spring under largely snow-free ice cover conditions. While there will always be a thin, stable conductive layer immediately below the ice, shortwave radiation will tend to destabilize the column beneath this (e.g., Jonas et al. 2003). Note that processes such as entrainment into the conductive layer from the convective layer below, as well as meltwater inflow, are neglected in this simplified treatment, even though they may influence the heat budget of the ice cover. The inclusion of such processes, as well as the benefits of increased resolution beneath the ice, await future model development.

The mixed layer model is more or less conventional (MacKay 2012, and references therein). Turbulent kinetic energy (TKE) in the mixed layer evolves based on a number of sources and sinks, the most important of which for our purposes is the mechanical energy flux F_q , due to buoyancy production and wind-driven stirring:

$$F_q = \frac{1}{2}(w_*^3 + c_n^3 u_*^3).$$

Here u_* is the surface friction velocity, c_n is a constant, and w_* is the convective velocity scale. The convective velocity scale, first proposed by Deardorff (1970), is determined from $w_*^3 = Bh$, where h is the mixed layer depth and B is the buoyancy flux:

$$B = \frac{g\alpha}{c_w\rho}H^*,$$

where g is the acceleration due to gravity, c_w is the specific heat capacity of water, α is the thermal expansivity

$$\alpha = -\frac{1}{\rho} \frac{\partial \rho}{\partial T} = \frac{2\beta\hat{T}}{(1 - \beta\hat{T}^2)},$$

and H^* is the "effective" surface heat flux (Rayner 1980)

$$H^* = -(L^* - H_S - H_E) - \left[Q^* + Q(h) - \frac{2}{h} \int_0^h Q dz \right].$$

This latter expression accounts for both surface fluxes (net longwave L^* , net shortwave Q^* , turbulent sensible heat H_S , and turbulent latent heat H_E), as well as shortwave radiation Q (a function of depth z) integrated over the mixed layer. Complete details can be found in MacKay (2012). Given our equation of state, the thermal expansivity is very small near the temperature of maximum density, so that buoyancy production nearly vanishes and mixed layer deepening is dominated by surface stirring. Close to (and following) ice-on, the buoyancy flux changes sign (i.e., becomes a sink of TKE) but is

generally small at this time. Following ice-on, the surface wind stress vanishes and the mixed layer depth is at a minimum. Mixed layer deepening due to the production of TKE in this way is here called forced convection to distinguish it from free convection arising from gravitational instability. The combination of forced and free convection largely determines the thermal structure of lakes near the time of ice-on and ice-off (Farmer and Carmack 1981).

2) SNOW AND ICE COVER

The model employs a simple staggered finite difference grid of fixed vertical resolution (0.5 m), apart from a thinner surface skin layer (0.05 m), which was included in order to facilitate faster interaction with the overlying atmosphere (MacKay 2012). Each layer is made up of liquid water, ice, or a combination of both, and its thermal properties—in particular, thermal conductivity and heat capacity—are linear combinations of those of water and ice as appropriate. The calculation of light availability at depth accounts for different extinction coefficients for water and ice, as well as the optical properties of snow cover if present (see below).

Ice forms in a model layer when the energy balance of the layer is sufficiently negative to cool it beyond 0°C, provided some liquid water still exists in the layer. If this is the case, the remaining liquid is brought to 0°C and any excess energy deficit is used to freeze some (or all) of it. If the energy balance of the layer is sufficiently positive and ice exists in the layer, then some energy is used to raise the temperature of the ice to 0°C (if necessary) and any remaining energy used for melting. In general, energy flux convergence in a layer is the result of thermal conduction and solar radiation extinction only. At the surface, of course, the energy balance includes turbulent heat and radiative exchange with the atmosphere (MacKay 2012), as well as the heat flux due to precipitation and thermal conduction from snow cover.

Fractional ice cover is a well-known feature of larger lakes subject to sufficient wind stress, which can mechanically break ice to produce pressure ridges and open water leads. The presence of some open water will alter turbulent and radiative flux exchange with the atmosphere, as well as light availability at depth due to differences in roughness, albedo, and light extinction between water and ice. Lepparanta and Wang (2008) present a scaling argument that suggests lake ice is stable to mechanical break up when

$$H_{\text{ice}}/L > 10^{-5},$$

where H_{ice} is the ice thickness and L is the maximum fetch. Since the CSLM does not represent lake shape, we

take L as the square root of the surface area, and for the 54-ha lake in this study, the limiting ice thickness $H_{\text{lim}} = 0.7$ cm. Thus, the period of fractional ice cover for this lake is likely very short, but this will be a considerably more important process for larger lakes (note that fractional snow cover is an important process for lakes of any size). When simulated ice thickness is less than H_{lim} , the fractional ice cover varies linearly as

$$F_{\text{ice}} = H_{\text{ice}}/H_{\text{lim}}.$$

If precipitation forcing data are available (i.e., either from an atmospheric model or observations), then snow cover can accumulate on the lake ice in the model. If the type of precipitation is unknown, then the model can partition the total precipitation into snowfall and rainfall based on near-surface air temperature in a number of different ways: here we simply assign the precipitation as entirely rainfall or entirely snowfall depending on whether the near-surface air temperature is above or below 0°C.

The snowpack physics module from CLASS (Verseghy 2016) has been added to the CSLM. The snowpack is simulated as a layer thermally separate from the underlying ice. The skin temperature of the snow is evaluated on the basis of the bulk snow temperature and the solution of the surface energy balance. The albedo of the snowpack decreases exponentially with time until refreshed by snowfall. The density of the snowpack increases exponentially with time (moderated by the addition of fresh snow) to a maximum value dependent on the snow depth and temperature. The fresh snow density is a function of the air temperature. The snow thermal conductivity depends on the snowpack density. Melting occurs when the skin temperature or the bulk snow temperature is projected to exceed 0°C, at which point the excess heat is used to melt part or all of the snowpack. Meltwater or rainfall percolates into the snowpack and refreezes until the pack is fully ripened to 0°C; subsequent fluxes of water become runoff. The snow cover is assumed to be complete until the snow depth falls below 0.10 m, after which it becomes patchy (the depth is held constant at 0.10 m and the snow cover is recalculated on the basis of conservation of mass). These processes, along with references, are summarized in Table 1.

A new snow-ice production scheme that conserves both mass and energy is now included in the model and is completely described in the appendix. In this scheme, a layer of snow is flooded by lake water when the underlying ice cannot support the weight of the snow, and this layer is assumed to freeze immediately and completely. In reality, neither is necessarily true: freezing may be delayed and slush layers have been observed even in midwinter. Later versions of the model

TABLE 1. Equations used for calculating snow properties, where z_s is snow depth (m), T_a is air temperature (K), and T_f is freezing temperature (K).

Snow property	Equation	Data source
Aging of snow albedo α_s	$\alpha_s(t+1) = [\alpha_s(t) - \alpha_{s,\text{old}}] \exp(-0.01\Delta t/3600) + \alpha_{s,\text{old}}$, where $\alpha_{s,\text{old}} = 0.50$ for melting snow and 0.70 otherwise	Aguado (1985), Robinson and Kukla (1984), and Dirmhirn and Eaton (1975)
Max snow density $\rho_{s,\text{max}}$ (kg m^{-3})	$\rho_{s,\text{max}} = A_s - (204.70/z_s)[1.0 - \exp(-z_s/0.673)]$, where $A_s = 700.0$ for melting snow and 450.0 otherwise	Tabler et al. (1990)
Aging of snow density ρ_s (kg m^{-3})	$\rho_s(t+1) = [\rho_s(t) - \rho_{s,\text{max}}] \exp(-0.01\Delta t/3600) + \rho_{s,\text{max}}$	Longley (1960) and Gold (1958)
Density of fresh snow $\rho_{s,i}$ (kg m^{-3})	$\rho_{s,i} = 67.92 + 51.25 \exp[(T_a - T_f)/2.59]$ for $T_a < T_f$ and $\rho_{s,i} = 119.17 + 20.0(T_a - T_f)$ for $T_a \geq T_f$	Hedstrom and Pomeroy (1998) and Pomeroy and Gray (1995)
Thermal conductivity λ_s ($\text{W m}^{-1} \text{K}^{-1}$)	$\lambda_s = 3.233 \times 10^{-6} \rho_s^2 - 1.01 \times 10^{-3} \rho_s + 0.138$ for $\rho_s \geq 156.0$ and $\lambda_s = 0.234 \times 10^{-3} \rho_s + 0.023$ for $\rho_s < 156.0$	Sturm et al. (1997)
Transmissivity τ_s	$\tau_s = \exp(-25.0z_s)$	Greenfell and Maykut (1977) and Thomas (1963)

will include an optional slush layer. It is worth noting that for the lake examined in this study, between 1980 and 2011 there were 54 surveys that measured snow, slush, and ice thickness, and of these only 18 (33%) indicated a nonzero amount of slush with a median value of only 6 cm (compared with 42 cm total ice). Latent heat from the freezing of the pore water is first used to warm the snow crystals in the slush layer to 0°C, with the remainder going into the overlying snowpack. The flood water is already at 0°C since it originates just below the ice. If the temperature of the snowpack is driven above the freezing point, then a portion is melted so that the snowpack temperature is restored to 0°C. Note that the snow-ice layer that forms is thicker than the snow layer that is consumed because of the thermal expansion of the freezing pore water, and this is accounted for in the scheme. In reality, the density of the snow-ice layer can be less than the density of conglomeration ice because of the presence of air bubbles—this process is currently not captured in this scheme. Both the snow-ice and conglomeration ice are assumed to be free of air bubbles. In addition, the transmissivity of the snow-ice is assumed to be the same as that for conglomeration ice for now—a potentially significant simplification that will need to be revisited in the future. Thus, the main impact of the snow-ice process is to remove snow from the overlying snowpack, add ice thickness, and warm the snow. The impact of changes in light penetration due to the presence of both unfrozen slush and snow-ice with different optical properties awaits future model developments. Nevertheless, the impact of this scheme on the mass and energy balance of the simulated snow and ice layers is dramatic, as will be shown below.

b. Experimental Lakes Area

The International Institute for Sustainable Development's ELA is a region of 58 lakes on the Boreal Shield of northwestern Ontario. Lake 239 (49°39.8'N,

93°43.4'W) is a 54-ha oligotrophic headwater lake at the ELA with a maximum depth of 31 m, a mean depth of 11 m, and shortwave extinction typically around 0.9 m^{-1} . Environment and Climate Change Canada has instrumented this lake in support of its numerical modeling research program since 2007. Lake bathymetry and instrumentation currently in use are indicated in Fig. 1.

1) IN SITU METEOROLOGICAL AND LIMNOLOGICAL DATA

Incoming and outgoing shortwave (SW) radiation, and incoming longwave (LW) radiation were measured at 10-min intervals from a raft deployed about 100 m from the southern shore of Lake 239 (Fig. 1). SW is measured using upward- and downward-facing Eppley Precision Spectral Pyranometers (PSPs), and incoming LW is measured with an upward-facing Eppley Precision Infrared Radiometer (PIR). Standard meteorology was observed from a short tower deployed near a small island near the eastern side of the lake (Fig. 1). Temperature and humidity (Campbell HMP45C), wind speed (RM Young), and barometric pressure (RM Young) were observed every 10 min at approximately 2 m above lake surface. These data along with the incoming LW and SW were used to drive the model, which also used a time step of 10 min. Temperature data were collected at hourly intervals using a string of HOBO Pendant temperature loggers (0.5° accuracy at 25°C), since October 2013. This string was deployed near the point of maximum depth of the lake, with sensors at 1, 2, 3, 4, 5, 6, 8, 10, and 28 m depth. Along with these data, snow and ice survey data routinely collected at ELA are also used in the evaluation of the CSLM below.

2) PRECIPITATION FORCING DATA

Accurate precipitation forcing is essential to properly simulate snow and ice processes but can be plagued with

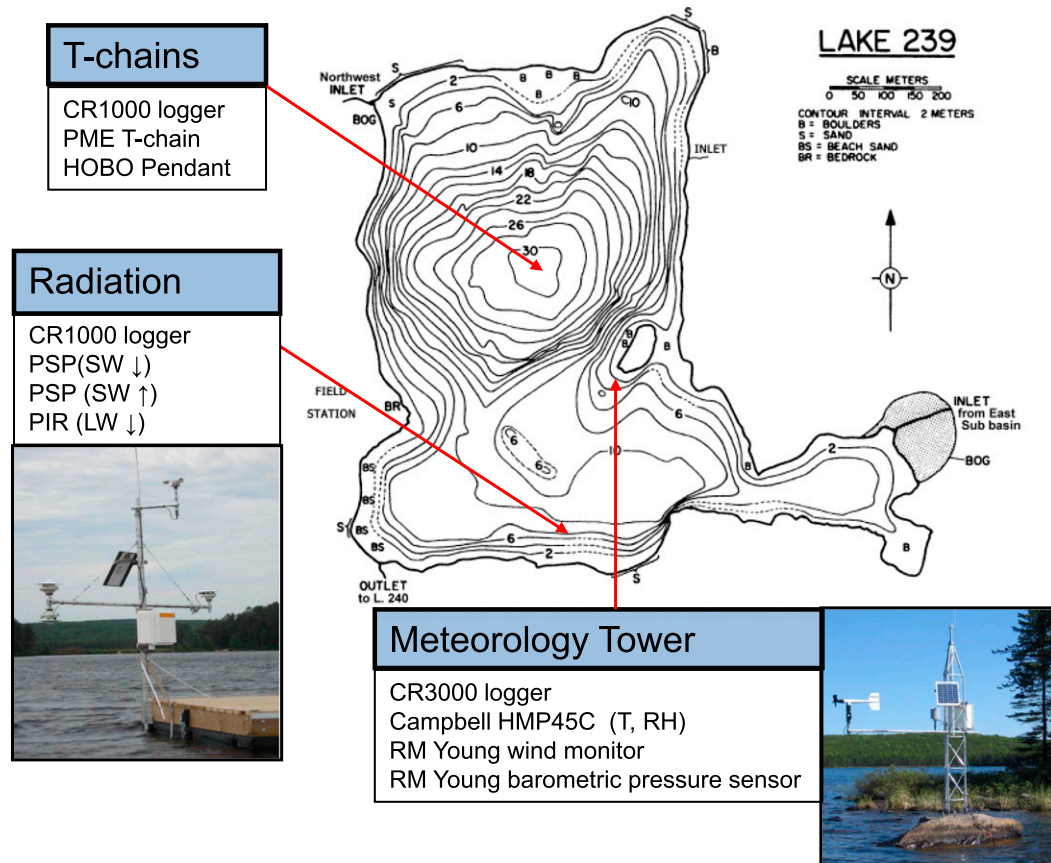


FIG. 1. Bathymetry of Lake 239 and instrumentation used in this study, with approximate locations on the map indicated.

difficulties, for example, related to the underestimation of solid precipitation in windy environments. An alternative to relying solely on precipitation gauge data is to use a precipitation analysis product, and here we employ the Regional Deterministic Precipitation Analysis (RDPA) from Environment and Climate Change Canada (http://collaboration.cmc.ec.gc.ca/cmc/cmci/product_guide/submenu/capa_e.html). This North American configuration of the Canadian Precipitation Analysis (CaPA) combines gauge and weather radar data with a short-term forecast from the numerical weather prediction Global Environmental Multiscale model (GEM) in its regional configuration using optimal interpolation and provides a best estimate of precipitation amounts on a 10-km grid every 6 h. Fortin et al. (2015a) successfully used CaPA–RDPA to simulate snow depth at a windy location in the forest–tundra ecotone.

In the vicinity of the ELA (within 100 km), there are only four operational stations reporting between 2013 and 2015: the Rawson lake reference climate station, the Kenora airport, the Kenora reference climate station, and the Dryden regional airport station. Precipitation

reports from these stations are combined with data from the Dryden weather radar and short-term forecasts from the GEM. For each 10-km grid cell of the analysis and each 6-h time step, the final estimate depends not only on the reports from the stations, the estimate from the radar, and the GEM forecast, but also on the distance of the grid cell to the stations, the gauge type, the wind shield used at the gauge, the precipitation type, and the weather radar and the weather forecast skill. The quality control algorithm and the optimal interpolation algorithm are documented in Lespinas et al. (2015) and Fortin et al. (2015b).

3. Results

a. Ice-on

The simulation for 2013–14 began on 16 July, but our analysis begins in the weeks leading up to ice-on. Ice-on was manually observed to occur on 22 November [day of year (DOY) 326], with the model first producing ice 3 days earlier on 19 November (Fig. 2a). The ice begins

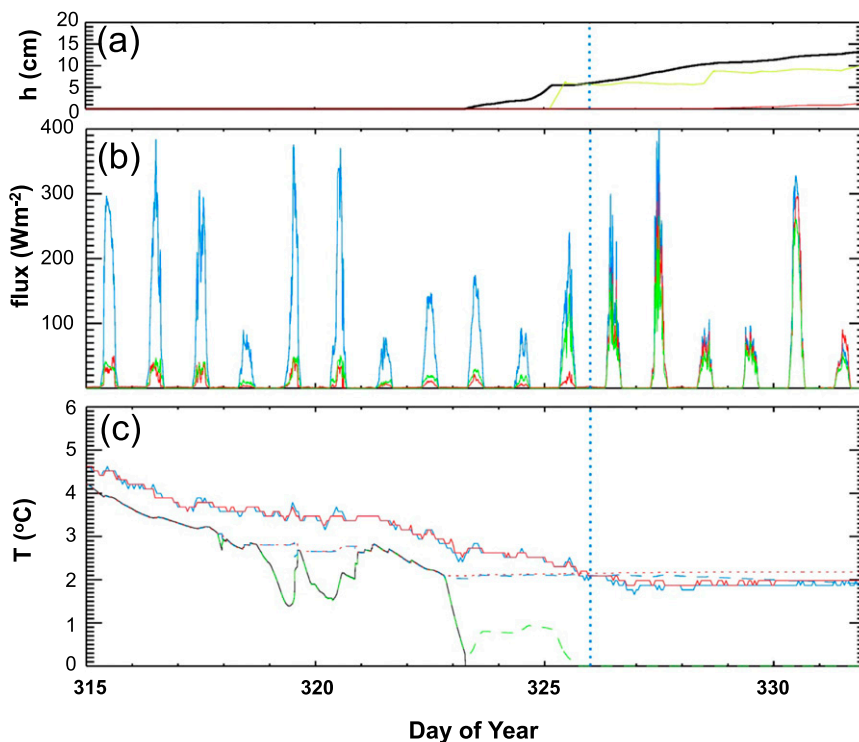


FIG. 2. Lake 239 ice-on for 2013: (a) simulated ice thickness (black), mean snow depth (green), and cumulative snow-ice (red); (b) observed incoming (blue) and outgoing (red) SW radiation and simulated outgoing SW radiation (green); (c) simulated skin (black), 0.5-m (green dash), 1-m (blue dash), and 2-m (red dash) temperature and observed 1-m (blue solid) and 2-m (red solid) temperature. The vertical dotted blue line represents manually observed ice-on.

accumulating a low-density snow cover on 21 November, but significant snow-ice production does not occur until later in the winter (see below); ice growth at this stage is entirely through congelation. Ice-on can be seen clearly from the large jump in observed outgoing SW radiation that occurred on 22 November, consistent with the manually determined ice-on date (Fig. 2b, red curve). In addition, it is evident that the model's open water albedo, as well as surface albedo (a weighted average of snow and bare ice albedo based on fractional snow cover) after observed ice-on both agree well with the observations.

Both the simulated and observed near-surface temperatures are well mixed prior to ice-on, though the simulation does show a cold bias, generally less than 1°C (Fig. 2c). After ice-on this bias is very small, and both the simulation and observations indicate the initiation of winter stratification. Based on the observed meteorological conditions, both the simulated (DOY 323) and observed (DOY 326) ice-on dates correspond with relatively calm winds and cold air temperatures, conditions amenable to the production of congelation ice (Fig. 3). Based on Fig. 3, it is possible that ice really did form on 19 November as the model suggests, but then melted the

next day when air temperatures rose above freezing. No melt, however, was simulated.

The 2014–15 simulation began 29 October (DOY 302), after overturn had already taken place but more than two weeks before ice-on. Figure 4 compares simulated temperature profiles with observations for both simulations near the time of ice-on. In both cases the model simulates cooling of the fully mixed lake well. Both simulations show that the lake is usually fully mixed in the weeks prior to ice-on, and this is borne out in the observations. Mixing is achieved by a combination of forced convection (indicated by the depth of the mixed layer in Fig. 4) and free convection (indicated by the dotted regions in Fig. 4). Forced convection is nearly entirely generated through wind stress: buoyancy production is virtually absent given that temperatures are close to the temperature of maximum density (not shown). There are some differences, however. In the days preceding ice-on in 2013, but after cooling below the temperature of maximum density, both forced and free convection are weaker and the simulated lake restratifies—a feature not evident in the observations (Figs. 4b,c, near DOY 320). A wind mixing event occurs the day before simulated ice-on, but this is insufficient to

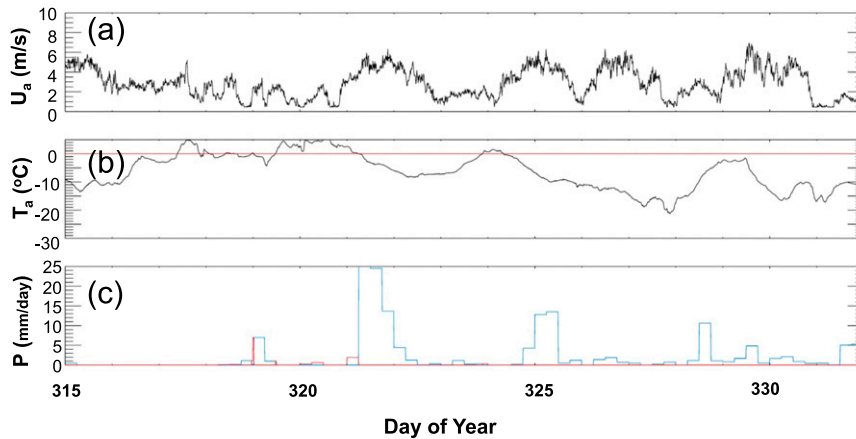


FIG. 3. Lake 239 meteorological forcing for the 2013 ice-on period: (a) 2-m wind speed, (b) 2-m air temperature, and (c) mean 6-hourly precipitation rate (rain, red; snow, blue).

mix the lake to the bottom, and once ice forms the lake remains stratified. Note that while forced convection ceases with the appearance of ice cover, Fig. 4 shows that free convection continues for several days while the ice and snow cover are sufficiently thin to allow the passage of SW radiation. In the case of 2013, however, this was insufficient to mix the lake to the bottom.

The ice-on process for 2014 is illustrated in Fig. 5 and appears rather less straightforward than the previous year. Ice-on was manually observed to have occurred on 21 November (DOY 325), but there is little signal of this in the observed outgoing SW radiation (Fig. 5b, red). The radiation data suggest that ice existed on and after 24 November (DOY 328), and perhaps during 16–17 November (DOY 320–321),

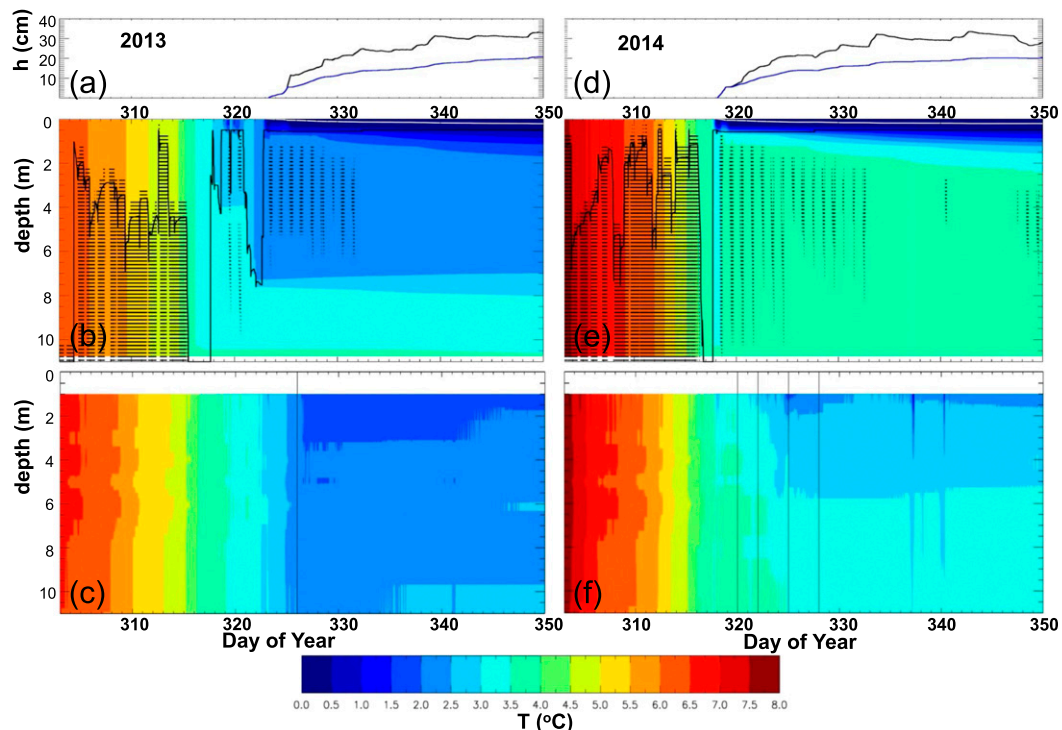


FIG. 4. The ice-on period from 30 Oct to 16 Dec (left) and (right) 2014. (a),(d) Simulated ice thickness (blue) and ice plus snow thickness (black); (b),(e) simulated temperature profiles (contoured), simulated mixed layer depth (solid black), and extent of free convection (black dots); and (c),(f) observed temperature profiles. Thin vertical lines in (c) and (f) delineate periods of possible ice-on as described in text.

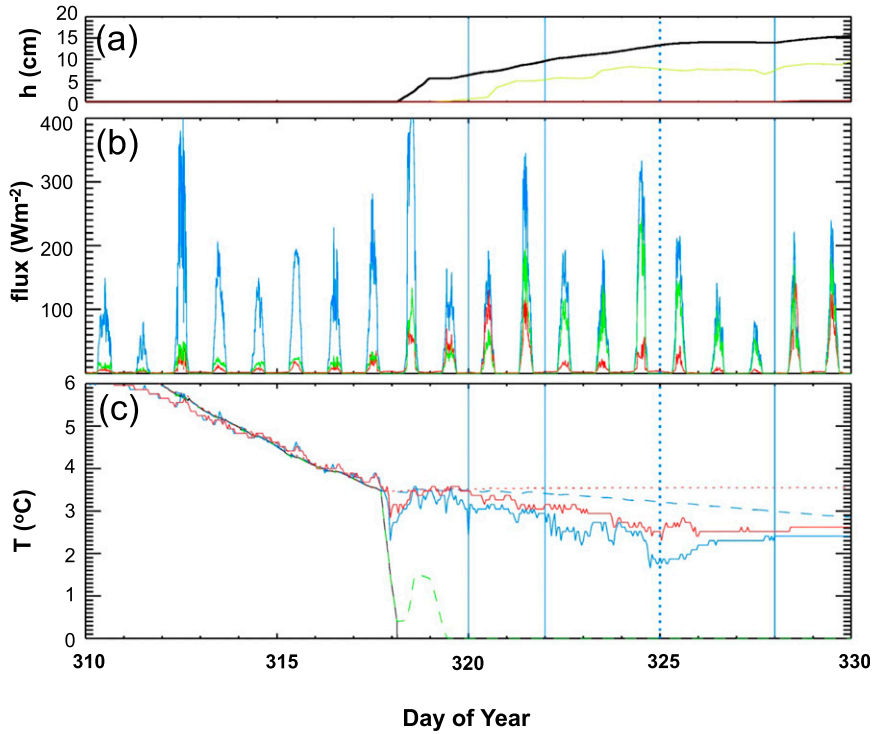


FIG. 5. As in Fig. 2, but for 2014. Thin vertical lines delineate periods of possible ice-on as described in text.

disappearing again by 18 November. In addition, the observed 1-m (and to some extent 2 m) temperatures show a reduction in variability, consistent with the formation of an ice cover, after about 22 November (DOY 326) and during 16–17 November (Fig. 5c). The model first simulates ice on 14 November (DOY 318), 2 days before the first observed signs of ice but up to 10 days before the likely final ice-on. Once again, both the simulated and observed 1- and 2-m temperatures show the initiation of winter stratification, but because the model

produced ice too early, thus severely limiting the lake’s ability to cool, the simulated temperatures are biased warm.

The radiation data suggest that 16–24 November (DOY 320–328) may be associated with ephemeral ice cover with periods of both production and melting. Meteorological data show that 16–21 November was cold, windy, and snowy, which likely would have produced very complicated surface conditions including frazil ice, a process not currently represented in the model (Fig. 6). The manually observed ice-on date

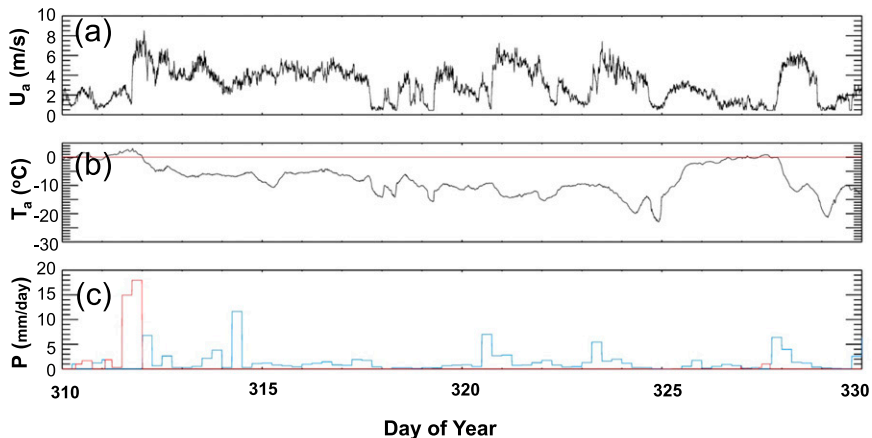


FIG. 6. As in Fig. 3, but for the 2014 ice-on period.

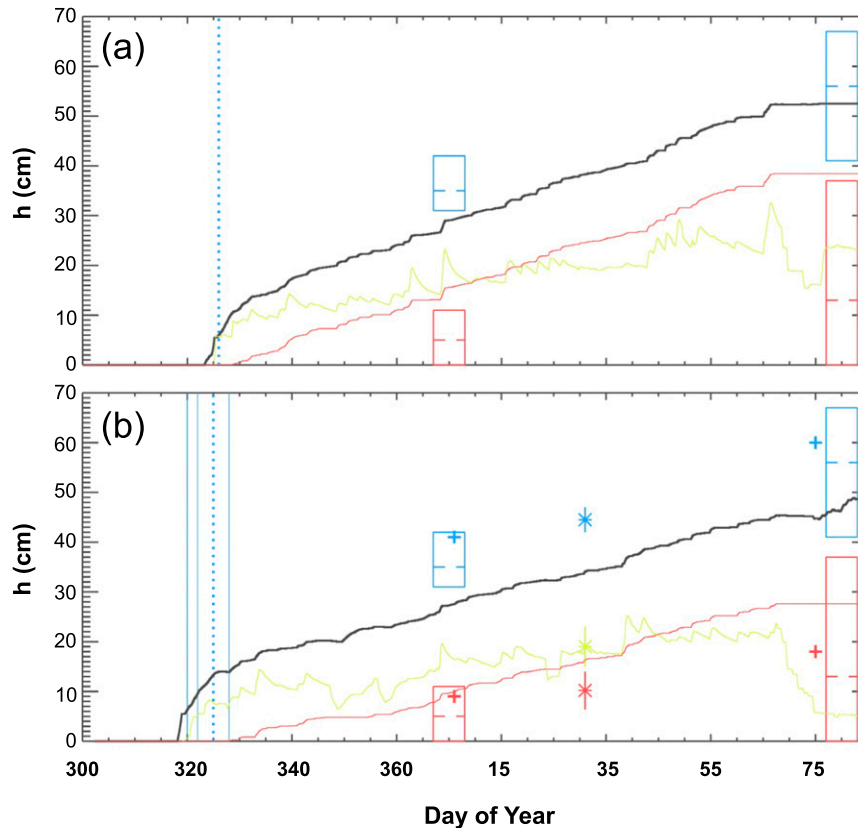


FIG. 7. Ice and mean snow thickness for (a) 2013–14 and (b) 2014–15: simulated mean snow depth (green), simulated cumulative snow-ice (red), and simulated total ice (black). No observations were made during 2013–14. ELA routine January and March surveys for 2015 are indicated by plus signs. Enhanced observations of ice thickness and snow depth were made on 31 Jan 2015 (asterisks with vertical lines indicating range). Min, max, and mean total ice (blue) and snow-ice (red) observations for 2007–12 (January and March) are indicated by boxes in (a) and (b).

(DOY 325) is clearly associated with very cold, calm conditions, but for the next 2 days temperatures warmed to near 0°C and any ice cover may have melted. Temperatures finally dropped again on 24 November, and the large increase in observed outgoing SW (Fig. 5b) suggests that this is the actual (final) ice-on date, as air temperatures did not approach freezing again for several weeks (not shown). The model produced ice cover a full 10 days before this, again during a period of cold, calm atmospheric conditions (Fig. 6), and failed to capture the intervening melt period. In fact, the observed 1- and 2-m water temperatures do show a sudden drop at this time (Fig. 5c), but they recover and continue a more gradual decline while the modeled lake surface cools rapidly to produce ice.

b. Ice growth and snow cover

Ice thickness, cumulative snow-ice, and mean snow-pack thickness throughout the winter growth period

are shown in Fig. 7 for both simulations. Snow and ice thickness measurements were not available for 2013–14, but minimum, maximum, and mean January and March ice thickness observations for 2007–12 are indicated as box plots in the figure to give a sense of recent climatology (total ice, blue; snow-ice, red). For both the 2013–14 and 2014–15 simulations, simulated ice thickness is slightly less than this climatology in January but within the range for March. For 2014–15 more detailed measurements were available, and it can be seen that the simulated ice thickness is about 25% too thin between early January and mid-March. On 31 January 2015, total ice thickness, snow-ice thickness, and snow depth were all measured at 30 different locations across the lake. The range of these measurements is indicated by the length of the vertical line through the plotted symbol, indicating a certain level of spatial variability in these parameters, even for a relatively small lake. By 31 January the simulated mean snow depth is within the range of

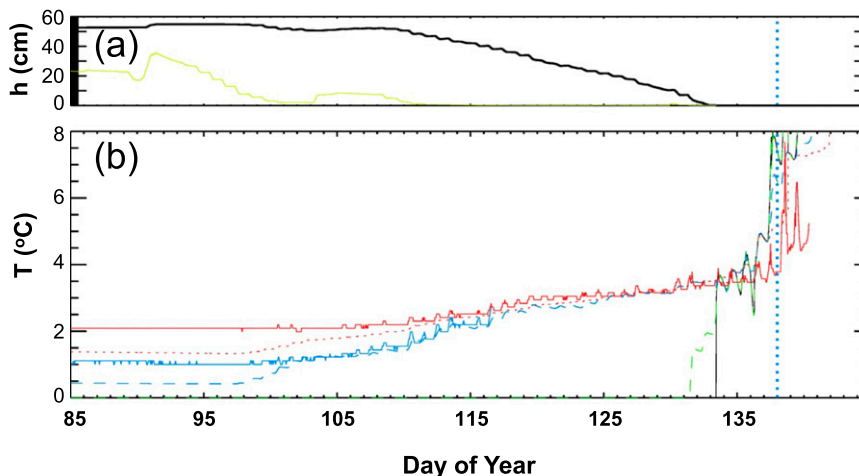


FIG. 8. As in Figs. 2a and 2c, but for ice-off in 2014.

measurements taken across the lake, and the simulated snow-ice is a few centimeters above the observed range (Fig. 7b). The total ice thickness, however, is clearly biased low. Snow-ice production begins about a week to 10 days after ice-on and continues until early March in both simulations. Snow-ice production is above or on the high side of climatology in the simulations, even though total ice is too thin. Note that the model produces snow-ice whenever the snow cover exceeds the carrying capacity of the ice. With the exception of melt, this is the only snowpack ablation process simulated, so that the snow water equivalent (SWE) is maintained at the critical threshold during the growth season (apart from rain or melt episodes). Observations on 31 January 2015 suggest that the observed snow cover is probably less than this threshold, suggesting that some snowpack ablation process not included in the model—for example, wind scouring—has taken place.

c. Snowmelt, ablation, and ice-off

Ice-off in 2014 was manually observed on 18 May (DOY 138) and simulated to occur about 5 days earlier (Fig. 8). Thus, the simulated ice cover duration for 2013–14 was 175 days, about 2 days shorter than observed. Outgoing SW radiation during ice-off would be expected to be complicated due to the presence of melt ponds, candle ice, etc., but the PSP data do not indicate any inconsistency with the manually observed date (not shown). Snow has largely disappeared by 20 April (DOY 110), after which ice melt begins in earnest (Fig. 8a). This is associated with lake warming below a depth of about 1 m, evident in both the simulation and the observations (Figs. 9b,c). In the model, mixing due to gravitational instability is active from 20 April until a few days after ice-off (Fig. 9b),

though the model indicates a weak, deepening thermocline while the observations do not. This mixing is clearly the result of SW radiation penetrating the ice following the elimination of snow cover and demonstrates how even a thin snow cover can affect lake thermal structure and mixing.

Manually observed ice-off in 2015 was on 27 April (DOY 117), and simulated ice-off was 6 days later (Fig. 10). Simulated ice cover duration was thus 170 days, 16 days longer than observed (based on a final ice-on date of 24 November). Ice melt does begin around 11 April (DOY 101) with the disappearance of the snowpack, but this is arrested for a few days with a fresh snowfall around 21 April (DOY 111). Meteorological data show that a 3-day precipitation event began on 19 April (DOY 109) that brought 8 mm of rain and 7 mm of snow (i.e., SWE) to the lake surface, during a period when air temperatures hovered close to 0°C (Fig. 11). Recall that the model assigns precipitation to snowfall for temperatures below freezing and rainfall for temperatures above, and assigning snowfall when rain actually occurred could have a negative impact on ice-off. Uncertainties in precipitation forcing and their impact on ice cover are discussed below.

However, examination of Fig. 9 indicates that problems with the simulation of ice-off may have originated well before 21 April. Comparison of Figs. 9b and 9c with Figs. 9e and 9f shows that the weeks leading up to ice-off were very different in 2015. Convective overturning in the model initially occurs in a deeper layer (roughly 5–9 m) in 2015 compared to 2014. Even though this convection started earlier, it was evidently not strong enough to overcome stability in the near-surface waters (i.e., around 1–4 m depth), which do show evidence of warming after the loss of snow cover around 2 April

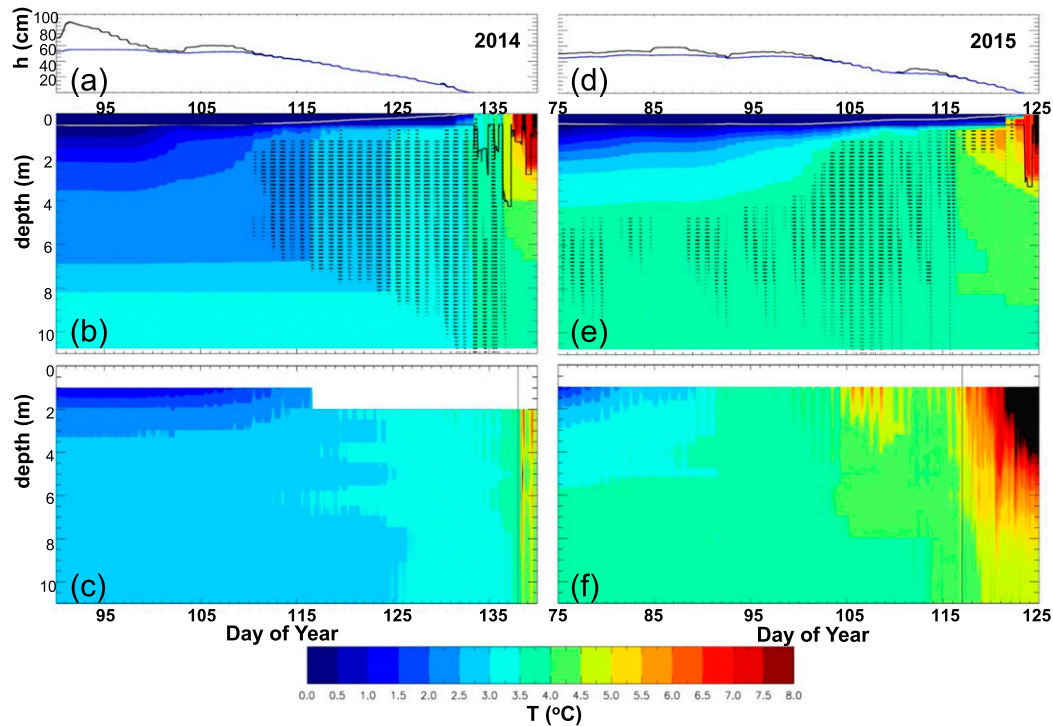


FIG. 9. As in Fig. 4, but for ice-off.

(DOY 92), but no mixing. The observations, however, show that temperature is well mixed, suggesting that convective mixing is likely occurring by this time (Fig. 9f). A key difference between this period and the corresponding mixing period from 2014 is that the mixing has occurred close to 4°C, and following this (beginning around DOY 99) the water begins to re-stratify near the surface because of the absorption of SW radiation that now acts to stabilize the column—all under the ice many days before ice-off. The simulation at

this time, however, now shows extensive mixing. In addition, a clear diurnal cycle is evident in observed temperatures above about 3 m depth that is absent in the simulation. The simulation does indicate restratification under the ice, but about 10 days late. Note that even during these restratification periods, as long as there is ice cover there must also coexist convective mixing between the top of the restratifying layer and the thin, stable layer beneath the ice (e.g., Kirillin and Terzhevik 2011), and this is also evident in Fig. 9e.

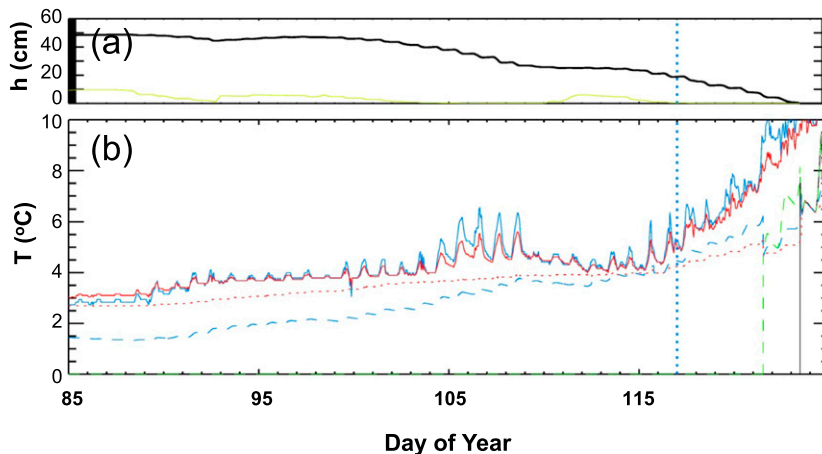


FIG. 10. As in Fig. 8, but for 2015.

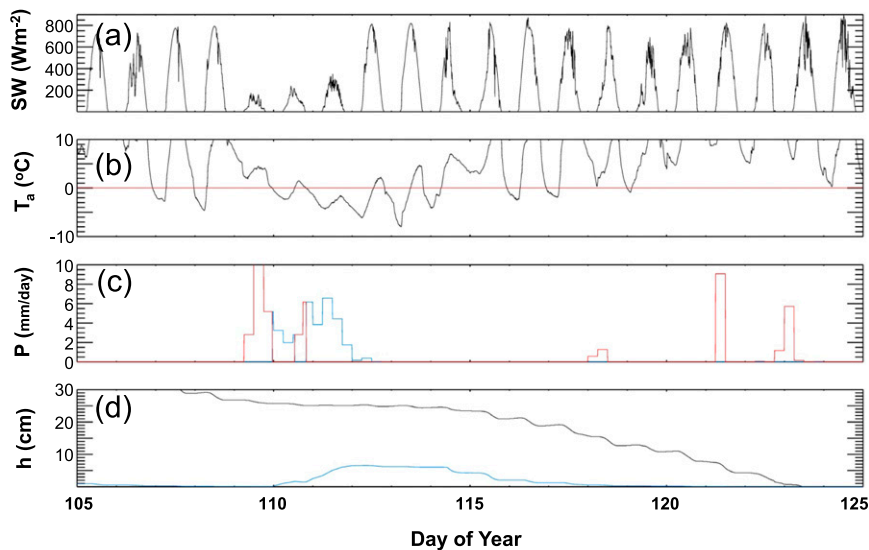


FIG. 11. Meteorology, ice, and snow cover during ablation and ice-off in 2015: (a) incoming SW radiation, (b) 2-m air temperature, (c) mean 6-hourly precipitation rate (rain, red; snow, blue), and (d) ice thickness (black) and mean snow depth (blue).

4. Sensitivity analysis

a. Snow-ice production and wind scouring

The importance of snow cover to ice phenology and thickness is well known and cannot be overstated. In regions with sufficient snowfall, the production of snow-ice affects ice thickness in two ways: directly through the flooding and freezing of a snow layer and indirectly through the removal of snow cover. In regions with sufficient snowfall that are sufficiently exposed (i.e., unsheltered by vegetation or topography), wind scouring of snow cover may also be an important mechanism for removing snow cover and thus affecting ice phenology and thickness. For example, in a detailed study of Alaskan lakes, [Sturm and Liston \(2003\)](#) found that snow properties (including SWE) were quite different over lakes compared with nearby tundra, and they attributed many of these differences to the influence of wind. The importance of wind scouring (and other wind effects) for lake ice in a forested boreal region such as the ELA is perhaps less obvious but cannot be ruled out without further study. As noted above, observations in [Fig. 7b](#) hint at the possibility of at least some midwinter snowpack ablation.

To explore this issue further, we repeat the 2014–15 simulation in a series of sensitivity experiments. In [Fig. 12a](#) we show our standard simulation of total ice, snow, and cumulative snow-ice for the entire winter season. As we have noted, the ice thickness evolves in a reasonable way but is generally about 25% too thin compared with observations. Compared with the

detailed observations on 31 January, we see that snow depth is simulated well and cumulative snow-ice is slightly high. Ice-off is late by 6 days (ice-on is not affected by snow processes in this model). When the snow-ice production process is turned off, we find that a very deep snowpack develops over the ice, leading to a much thinner ice cover ([Fig. 12b](#)). As it turns out, the ice-off date is actually improved, so if one were evaluating the quality of the simulation based only on this observation, one would be misled into thinking the simulation was quite good when clearly the snow and ice simulations are substantially degraded.

In the absence of a snow-ice production mechanism, the simulated snow cover is simply too deep for a realistic ice cover to develop. However, one can improve the situation by simply “scouring” sufficient snow. For example, removing 62.5% of snowfall (i.e., assuming it blows off the lake as soon as it has fallen) leads to the simulation shown in [Fig. 12c](#). In this case, while the ice-off date has not improved compared with the standard simulation, the ice thickness has. However, we discourage such “tuning” of processes that are so poorly understood in order to improve individual results, especially for models intended for global application, and suggest that our standard simulation represents the best compromise.

b. Meteorological forcing uncertainty

While process uncertainty is certainly a source of error in any numerical model, even a perfect lake model may produce poor results when forced with poor-quality

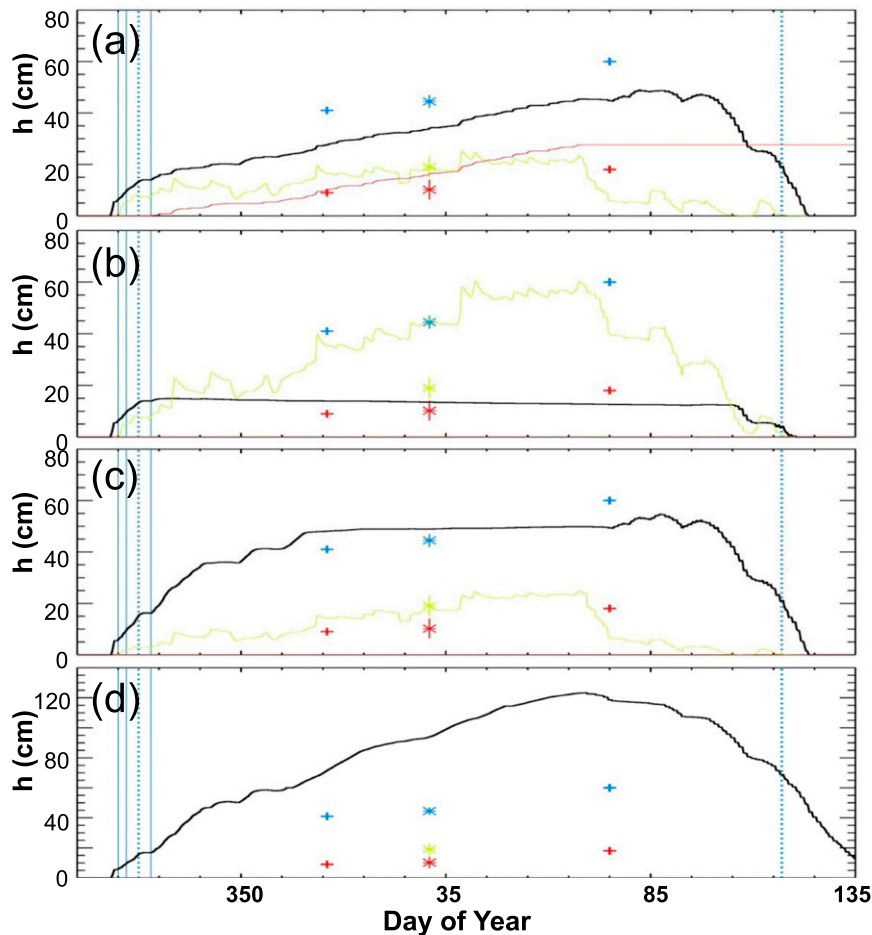


FIG. 12. Simulation sensitivity experiments for 2014–15: (a) standard simulation, (b) snow-ice process turned off, (c) snow-ice turned off with 62.5% snowfall removal due to wind scouring, and (d) no precipitation. Curves and plot symbols as defined in Fig. 7.

meteorological data. Errors can exist in all seven meteorological forcing fields required by any comprehensive surface model (lake or land): precipitation, incoming SW and LW radiation, wind speed, temperature, humidity, and pressure. Of particular relevance to this study is the quality of precipitation forcing data, given the importance of snow cover to the simulation of ice. While summer rainfall observations are relatively straightforward, wintertime precipitation measurements are notoriously difficult and, especially with the advent of more and more unmanned weather stations, not infrequently absent altogether. It is obviously not possible to simulate ice cover in a region such as the ELA without snowfall measurements: Fig. 12d shows a simulation for 2014–15 that includes no precipitation forcing. In this case more than 1.2 m of congelation ice grows, and ice-off is late by more than 3 weeks. Even when precipitation amount is carefully measured, uncertainties in precipitation type for any given event

remain. Consider the 15-mm mixed rain–snow event that occurred on 19 April (DOY 109; Fig. 11). Changing this single event to entirely rainfall improves the ice-off date by 1 day (not shown). Changing all of the precipitation that fell after 2 April to rain improves the ice-off date by an additional day (not shown).

5. Discussion

It is well known that the presence and nature of snow cover has a dramatic impact on lake ice. In our simulation of 2014–15 without precipitation forcing, the ice grew through congelation about twice as thick as observations indicated, with a concomitant error in ice-off of several weeks. Even changing the phase of precipitation during one or two springtime events had a measureable impact on ice-off date. It is clear that the quality of precipitation forcing—whether observed or modeled—is important for wintertime lake modeling.

Once snow has fallen, its evolution is also important. In our simulation of 2014–15 with precipitation but without snow-ice production, we found a very thin layer of ice covered with a very deep layer of snow. We could tune this simulation: by removing 62.5% of the snowfall—ostensibly through wind redistribution of the freshly fallen snow—we could improve our ice thickness simulation (though in this case not the ice-off date). In fact, blowing snow redistribution from open areas is an active area of research (e.g., [Sturm 2015](#), section 3.6) and may well be an important process for lakes in some cases. However, much more research is required, we feel, before sensible parameterizations can be developed for lake models intended for regional and/or global application. Even our simple representation of snow-ice production along with no wind redistribution produced reasonable simulations, at least for this relatively sheltered boreal lake.

It is evident that the weeks preceding ice-off were very different in 2014 compared with 2015. In 2014 the model shows, and the observations suggest, that a deep layer of convective mixing below 1 m existed for 3 weeks prior to ice-off. In 2015 convective mixing was simulated much deeper (below 5 m) than the observations initially suggest ([Figs. 9e,f](#)). By the time this convective layer reached 1 m depth, the observations show that the lake had already restratified (below the ice) with significant diurnal heating evident—heating that must have contributed to ice melt. The model also indicates restratification beneath the ice eventually, but about 10 days late. It seems likely that, had deep convective mixing occurred below 1 m earlier in the simulation, the 6 day bias in ice-off would have been improved.

Because energy fluxes are so small when ice is present, thermal conditions under ice cover are largely established prior to and during the ice-on process (e.g., [Farmer and Carmack 1981](#)). Thus, errors in the ice-on process could in fact impact ice-off many months later. [Figures 9e and 9f](#) show that in 2015 near-surface water is simulated too cold and is thus too stably stratified for penetrating SW to drive convective instability. However, [Fig. 5](#) shows that, because ice-on was simulated too early in 2014, simulated 1- and 2-m temperatures are actually too warm in the early days following ice-on. To examine this further, we calculated the heat content between 1 and 10 m based on the observed and simulated temperature profiles under ice cover. As expected, the heat contents in both observations and simulations changed very slowly but, unexpectedly, in different senses. Between DOY 330 and DOY 65 (100 days) the observed change in heat content was $9.68 \times 10^6 \text{ J m}^{-2}$ while that simulated was $-1.59 \times 10^7 \text{ J m}^{-2}$. The simulated bias of $-2.56 \times 10^7 \text{ J m}^{-2}$ corresponds to an

average energy flux error of about -3 W m^{-2} . A similar calculation for 2013–14 suggests an error of about -2.5 W m^{-2} . Interestingly, this is about the same magnitude as might be expected from wintertime sediment heat flux, at least during the early part of the ice season (e.g., [Rizk et al. 2014](#), and references therein). The role of sediment heat flux in the wintertime thermal structure and ice phenology of lakes in the current modeling context certainly warrants further study.

6. Conclusions

We have incorporated the complete snow physics package of the Canadian Land Surface Scheme (CLASS) and have added a new snow-ice production scheme to the Canadian Small Lake Model (CSLM). Detailed meteorological and limnological forcing and evaluation data have been acquired and two wintertime simulations of a small boreal lake in northwestern Ontario have been analyzed, with particular attention paid to lake thermal structure, snow and ice cover, and ice phenology.

Ice-on was simulated 3 days early in the 2013–14 simulation. Ice-on bias was probably larger in the 2014–15 simulation, though there is some uncertainty as to when ice-on actually occurred. The model first produced ice about 2 days before the first signs of ice in our SW radiometer data but a full 10 days before our best guess at final ice-on. An intervening melt period was not simulated. Strong winds, cold air temperatures, and snowy conditions must have led to complex surface conditions during this time, and we suggest the addition of frazil ice production in the model would be beneficial.

Total ice thickness and snow-ice thickness were close to or within recent climatology for both years, but more detailed observations during 2015 suggest a bias in total ice of about -25% . An extensive late January 2015 survey indicates that while the simulated ice cover was too thin, snow cover and snow-ice were close to observed.

Ice-off was about 5 days early in the 2013–14 simulation, resulting in a total ice cover season of 175 days, 2 days shorter than observed. Ice-off in the 2014–15 simulation was 6 days later than observed. Ice cover duration in this simulation was 170 days, up to 16 days longer than observed. Deep convective mixing (and subsequent restratification) under ice was about 10 days too late in this simulation, and this likely played a role in the delayed ice-off.

The important role of snow cover is clearly demonstrated in our simulations. A simple snow-ice production scheme, along with the snow physics parameterization of CLASS and a carefully constructed precipitation forcing dataset, have led to reasonable simulations of ice cover in our model. Turning off snow-ice production led

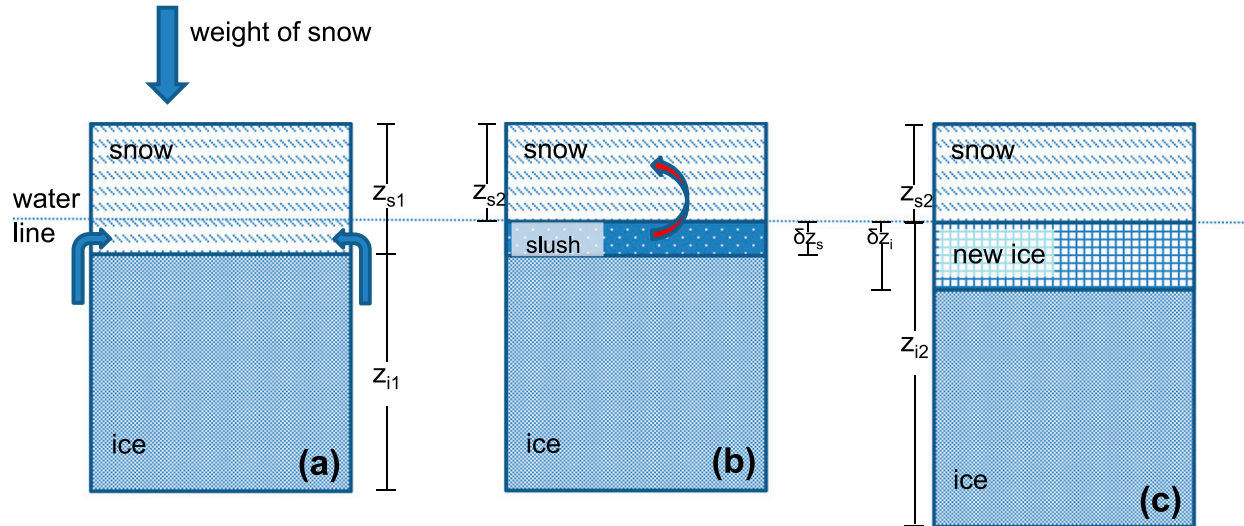


FIG. A1. The process of snow-ice formation in the CSLM: (a) ice cannot support the weight of overlying snow so that water floods a thin layer of snow to form slush, (b) slush layer freezes releasing latent heat into the overlying snow layer, and (c) new snow-ice is thicker than slush layer due to thermal expansion.

to a much degraded simulation without the ad hoc removal of a large fraction (62.5%) of snowfall.

While the CSLM is well suited for detailed year-round simulations of individual lakes, one of its primary roles will be to serve as a component within the land surface modules of Environment and Climate Change Canada's various global and regional climate and numerical weather prediction systems. Progress toward this end is outlined in Verseghy and MacKay (2017).

Acknowledgments. Chandra Rodgers organized and maintained the temperature data used in this analysis. ELA staff, especially Lee Hrenchuk, Ken Sandilands, and Ken Beaty have provided ongoing and invaluable assistance throughout this research program. An anonymous reviewer provided an exceptionally thorough reading and helpful comments for which we are grateful.

APPENDIX

Snow-Ice Production

The production of snow-ice in the CSLM is outlined here. When the weight of overlying snow exceeds the carrying capacity of the ice, cracks will form in the ice and liquid lake water will flood a layer of snow. This occurs when

$$z_{s1}\rho_s > z_{i1}(\rho_w - \rho_i), \quad (\text{A1})$$

where ρ_s , ρ_w , and ρ_i are the densities of snow, liquid water, and ice, and z_{s1} and z_{i1} are the initial snow and ice thicknesses (z_{s2} and z_{i2} , below, are the final snow and ice

thicknesses, respectively). This is the situation shown in Fig. A1a. The flooded layer has thickness

$$\delta z_s = z_{s1} - z_{s2}$$

and is made up of snow-ice crystals and liquid water (i.e., slush). The mass of water δM_l drawn into the snow layer depends on the pore volume of the snow

$$\theta = \frac{\rho_i - \rho_s}{\rho_i},$$

(where we have neglected the density of air compared to water and snow) so that

$$\delta M_l = \rho_w \theta \delta z_s. \quad (\text{A2})$$

In this scheme all of the liquid water drawn into the slush layer is assumed to freeze. Some of the latent heat generated when this mass freezes goes into heating the snow in the slush layer to 0°C , with the remainder going into the overlying snow (Fig. A1b), which warms and may also undergo some melting. The new ice layer that forms is thicker than the depth of snow consumed, due to the thermal expansion of the freezing liquid water in the slush layer. From the conservation of mass,

$$\rho_i \delta z_i = [\rho_w \theta + \rho_i(1 - \theta)] \delta z_s, \quad (\text{A3})$$

where $\delta z_i = z_{i2} - z_{i1}$ is the thickness of the new ice layer (Fig. A1c). In this version of the model, the entire pore space is filled with water before freezing. In reality, a fraction of the pore space is retained, and snow-ice

generally contains air bubbles. This tends to reduce both the density and transmissivity of snow-ice compared to congelation ice.

It will prove convenient to define a slush expansion factor α from (A3) as

$$\alpha = \frac{\delta z_i}{\delta z_s} = \frac{[\rho_w \theta + \rho_i(1 - \theta)]}{\rho_i}$$

as well as an ice capacity factor η [based on (A1)] as

$$\eta = \frac{z_{s2}}{z_{i2}} = \frac{\rho_w - \rho_i}{\rho_s}$$

The problem is now solved by assuming the final snow cover z_{s2} exactly balances the carrying capacity of the final ice thickness z_{i2} . From (A3),

$$z_{i2} = z_{i1} + \alpha(z_{s1} - z_{s2}),$$

but

$$\begin{aligned} z_{s2}\rho_s &= z_{i2}(\rho_w - \rho_i) \\ \Rightarrow z_{s2} &= \eta z_{i2} \\ &= \eta[z_{i1} + \alpha(z_{s1} - z_{s2})] \\ &= \eta z_{i1} + \eta\alpha z_{s1} - \eta\alpha z_{s2} \\ &= \frac{\eta(z_{i1} + \alpha z_{s1})}{1 + \alpha\eta} \end{aligned}$$

and

$$z_{i2} = \frac{z_{s2}}{\eta} = \frac{(z_{i1} + \alpha z_{s1})}{1 + \alpha\eta}.$$

The latent heat generated by this process is simply

$$Q_L = L_f \delta M_i = \rho_w L_f \theta \delta z_s,$$

where L_f is the latent heat of fusion. The distribution of this heat depends on the initial temperature T_{s1} of the snowpack. Some of this heat is consumed by snow crystals in the slush layer that are warmed to $T^* = 273.15$ K, the temperature at which freezing is assumed to occur. This heat is given by

$$Q_{\text{warm}} = \rho_s c_p (T^* - T_{s1}) \delta z_s,$$

where $\rho_s c_p$ is the volumetric heat capacity of the snow. The remainder of the heat warms the remaining snowpack, which increases in temperature by an amount

$$\delta T_s = \frac{Q_L - Q_{\text{warm}}}{\rho_s c_p Z_{s2}}.$$

If this drives the temperature of the snowpack above zero, the snow temperature is restored to zero with the remaining heat used for melting snow.

REFERENCES

- Aguado, E., 1985: Radiation balances of melting snow covers at an open site in the central Sierra Nevada, California. *Water Resour. Res.*, **21**, 1649–1654, doi:10.1029/WR021i011p01649.
- Cheng, B., J. Launianen, and T. Vihma, 2003: Modelling of superimposed ice formation and sub-surface melting in the Baltic Sea. *Geophysica*, **39**, 31–50.
- Deardorff, J., 1970: Convective velocity and temperature scales for the unstable planetary boundary layer and for Rayleigh convection. *J. Atmos. Sci.*, **27**, 1211–1213, doi:10.1175/1520-0469(1970)027<1211:CVATSF>2.0.CO;2.
- de Stasio, B. T., A. Joice, K. Prescott, G. Gal, D. P. Hamilton, and L. G. Rudstam, 2016: Comparisons of water clarity and climate warming effects on hydrodynamics of Oneida Lake: Applications of a dynamic reservoir model. *Oneida Lake: Long Term Dynamics of a Managed Ecosystem and Its Fisheries*, L. G. Rudstam et al., Eds., American Fisheries Society, 245–275.
- Dirmhirn, I., and F. D. Eaton, 1975: Some characteristics of the albedo of snow. *J. Appl. Meteor.*, **14**, 375–379, doi:10.1175/1520-0450(1975)014<0375:SCOTAO>2.0.CO;2.
- Duguay, C. R., G. M. Flato, M. O. Jeffries, P. Ménard, K. Morris, and W. R. Rouse, 2003: Ice-cover variability on shallow lakes at high latitudes: Model simulations and observations. *Hydrol. Processes*, **17**, 3465–3483, doi:10.1002/hyp.1394.
- Elo, A.-R., and S. Vavrus, 2000: Ice modelling calculations, comparison of the PROBE and LIMNOS models. *Verh. Int. Ver. Theor. Angew. Limnol.*, **27**, 2816–2819.
- Farmer, D. M., and E. Carmack, 1981: Wind mixing and re-stratification in a lake near the temperature of maximum density. *J. Phys. Oceanogr.*, **11**, 1516–1533, doi:10.1175/1520-0485(1981)011<1516:WMARIA>2.0.CO;2.
- Flato, G. M., and R. D. Brown, 1996: Variability and climate sensitivity of landfast Arctic sea ice. *J. Geophys. Res.*, **101**, 25 767–25 777, doi:10.1029/96JC02431.
- Fortin, V., M. Jean, R. Brown, and S. Payette, 2015a: Predicting snow depth in a forest–tundra landscape using a conceptual model allowing for snow redistribution and constrained by observations from a digital camera. *Atmos.–Ocean*, **53**, 200–211, doi:10.1080/07055900.2015.1022708.
- , G. Roy, N. Donaldson, and A. Mahidjiba, 2015b: Assimilation of radar quantitative precipitation estimations in the Canadian Precipitation Analysis (CaPA). *J. Hydrol.*, **531**, 296–307, doi:10.1016/j.jhydrol.2015.08.003.
- Gold, L. W., 1958: Changes in a shallow snow cover subject to a temperate climate. *J. Glaciol.*, **3**, 218–222, doi:10.1017/S002214300002428X.
- Grenfell, T. C., and G. A. Maykut, 1977: The optical properties of ice and snow in the Arctic Basin. *J. Glaciol.*, **18**, 445–463, doi:10.1017/S0022143000021122.
- Hedstrom, N. R., and J. W. Pomeroy, 1998: Measurements and modelling of snow interception in the boreal forest. *Hydrol. Processes*, **12**, 1611–1625, doi:10.1002/(SICI)1099-1085(199808/09)12:10:11<1611::AID-HYP684>3.0.CO;2-4.
- Jonas, T., A. Y. Terzhevik, D. V. Mironov, and A. Wuest, 2003: Radiatively driven convection in an ice-covered lake investigated by using temperature microstructure technique. *J. Geophys. Res.*, **108**, 3183, doi:10.1029/2002JC001316.

- Keitzl, T., J. P. Mellado, and D. Notz, 2016: Impact of thermally driven turbulence on the bottom melting of ice. *J. Phys. Oceanogr.*, **46**, 1171–1187, doi:10.1175/JPO-D-15-0126.1.
- Kheyrollah Pour, H., C. R. Duguay, A. Martynov, and L. C. Brown, 2012: Simulation of surface temperature and ice cover of large northern lakes with 1-D models: A comparison with MODIS satellite data and in situ measurements. *Tellus*, **64A**, 17 614, doi:10.3402/tellusa.v64i0.17614.
- Kirillin, G., and A. Terzhevik, 2011: Thermal instability in freshwater lakes under ice: Effect of salt gradients or solar radiation? *Cold Reg. Sci. Technol.*, **65**, 184–190, doi:10.1016/j.coldregions.2010.08.010.
- , and Coauthors, 2012: Physics of seasonally ice-covered lakes: A review. *Aquat. Sci.*, **74**, 659–682, doi:10.1007/s00027-012-0279-y.
- Lepparanta, M., and K. Wang, 2008: The ice cover on small and large lakes: Scaling analysis and mathematical modelling. *Hydrobiologia*, **599**, 183–189, doi:10.1007/s10750-007-9201-3.
- Lepinas, F., V. Fortin, G. Roy, P. F. Rasmussen, and T. Stadnyk, 2015: Performance evaluation of the Canadian Precipitation Analysis. *J. Hydrometeorol.*, **16**, 2045–1064, doi:10.1175/JHM-D-14-0191.1.
- Longley, R. W., 1960: Snow depth and snow density at Resolute, Northwest Territories. *J. Glaciol.*, **3**, 733–738, doi:10.1017/S0022143000018037.
- MacKay, M. D., 2012: A process-oriented small lake scheme for coupled climate modelling applications. *J. Hydrometeorol.*, **13**, 1911–1924, doi:10.1175/JHM-D-11-0116.1.
- , and Coauthors, 2009: Modeling lakes and reservoirs in the climate system. *Limnol. Oceanogr.*, **54**, 2315–2329, doi:10.4319/lo.2009.54.6_part_2.2315.
- Magee, M. R., C. H. Wu, D. M. Robertson, R. C. Lathrop, and D. P. Hamilton, 2016: Trends and abrupt changes in 104 years of ice cover and water temperature in a dimictic lake in response to air temperature, wind speed, and water clarity drivers. *Hydrol. Earth Syst. Sci.*, **20**, 1681–1702, doi:10.5194/hess-20-1681-2016.
- Ménard, P., C. R. Duguay, G. M. Flato, and W. R. Rouse, 2002: Simulation of ice phenology on Great Slave Lake, Northwest Territories, Canada. *Hydrol. Processes*, **16**, 3691–3706, doi:10.1002/hyp.1230.
- Mironov, D., A. Terzhevik, G. Kirillin, T. Jonas, J. Malm, and D. Farmer, 2002: Radiatively driven convection in ice-covered lakes: Observations, scaling, and a mixed layer model. *J. Geophys. Res.*, **107**, 3032, doi:10.1029/2001JC000892.
- Oveisy, A., and L. Boegman, 2014: One-dimensional simulation of lake and ice dynamics during winter. *J. Limnol.*, **73**, 441–453, doi:10.4081/jlimnol.2014.903.
- Patterson, J., and P. Hamblin, 1988: Thermal simulation of a lake with winter ice cover. *Limnol. Oceanogr.*, **33**, 323–338, doi:10.4319/lo.1988.33.3.0323.
- Pomeroy, J. W., and D. M. Gray, 1995: Snowcover accumulation, relocation and management. National Hydrology Research Institute Science Rep. 7, Environment Canada, 144 pp.
- Rayner, K. N., 1980: Diurnal energetics of a reservoir surface layer. Environmental Dynamics Rep. ED-80-005, University of Western Australia, 227 pp.
- Rizk, W., G. Kirillin, and M. Lepparanta, 2014: Basin-scale circulation and heat fluxes in ice-covered lakes. *Limnol. Oceanogr.*, **59**, 445–464, doi:10.4319/lo.2014.59.2.0445.
- Robinson, D. A., and G. Kukla, 1984: Albedo of a disappearing snow cover. *J. Climate Appl. Meteor.*, **23**, 1626–1634, doi:10.1175/1520-0450(1984)023<1626:AOADSC>2.0.CO;2.
- Rogers, C. K., G. A. Lawrence, and P. F. Hamblin, 1995: Observations and numerical simulation of a shallow ice-covered midlatitude lake. *Limnol. Oceanogr.*, **40**, 374–385, doi:10.4319/lo.1995.40.2.0374.
- Semmler, T., B. Cheng, Y. Yang, and L. Rontu, 2012: Snow and ice on Bear Lake (Alaska)—Sensitivity experiments with two lake ice models. *Tellus*, **64A**, 17 339, doi:10.3402/tellusa.v64i0.17339.
- Sturm, M., 2015: White water: Fifty years of snow research in WRR and the outlook for the future. *Water Resour. Res.*, **51**, 4948–4965, doi:10.1002/2015WR017242.
- , and G. E. Liston, 2003: The snow cover on lakes of the Arctic coastal plain of Alaska, U.S.A. *J. Glaciol.*, **49**, 370–380, doi:10.3189/172756503781830539.
- , J. Holmgren, M. König, and K. Morris, 1997: The thermal conductivity of seasonal snow. *J. Glaciol.*, **43**, 26–41, doi:10.1017/S0022143000002781.
- Tabler, R. D., C. S. Benson, B. W. Santana, and P. Ganguly, 1990: Estimating snow transport from wind speed records: Estimates versus measurements at Prudhoe Bay, Alaska. *Proc. 58th Western Snow Conf.*, Sacramento, CA, Western Snow Conference, 61–78. [Available online at <https://westernsnowconference.org/node/620>.]
- Thomas, C. W., 1963: On the transfer of visible radiation through sea ice and snow. *J. Glaciol.*, **34**, 481–484, doi:10.1017/S0022143000027921.
- Vavrus, S. J., R. H. Wynne, and J. A. Foley, 1996: Measuring the sensitivity of southern Wisconsin lake ice to climate variations and lake depth using a numerical model. *Limnol. Oceanogr.*, **41**, 822–831, doi:10.4319/lo.1996.41.5.0822.
- Verseghy, D. L., 2016: CLASS—The Canadian Land Surface Scheme (version 3.6.3) technical documentation. Climate Research Division Internal Rep., Environment and Climate Change Canada, 176 pp.
- , and M. D. MacKay, 2017: Offline implementation and evaluation of the Canadian Small Lake Model with the Canadian Land Surface Scheme over western Canada. *J. Hydrometeorol.*, **18**, 1563–1582, doi:10.1175/JHM-D-16-0272.1.
- , R. D. Brown, and L. Wang, 2017: Evaluation of CLASS snow simulation over eastern Canada. *J. Hydrometeorol.*, **18**, 1205–1225, doi:10.1175/JHM-D-16-0153.1.
- Yang, Y., M. Lepparanta, B. Cheng, and Z. Li, 2012: Numerical modelling of snow and ice thicknesses in Lake Vanajavesi, Finland. *Tellus*, **64A**, 17 202, doi:10.3402/tellusa.v64i0.17202.